LETTERS

RAS–RAF–MEK-dependent oxidative cell death involving voltage-dependent anion channels

Nicholas Yagoda[1]*, Moritz von Rechenberg[3]*, Elma Zaganjor[1]*, Andras J. Bauer[1], Wan Seok Yang[1],
Daniel J. Fridman[1], Adam J. Wolpaw[1], Inese Smukste[1], John M. Peltier[3], J. Jay Boniface[3], Richard Smith[4],
Stephen L. Lessnick[4,5], Sudhir Sahasrabudhe[3] & Brent R. Stockwell[1,2]

Therapeutics that discriminate between the genetic makeup of normal cells and tumour cells are valuable for treating and understanding cancer. Small molecules with oncogene-selective lethality may reveal novel functions of oncoproteins and enable the creation of more selective drugs[1]. Here we describe the mechanism of action of the selective anti-tumour agent erastin, involving the RAS–RAF–MEK signalling pathway functioning in cell proliferation, differentiation and survival. Erastin exhibits greater lethality in human tumour cells harbouring mutations in the oncogenes *HRAS*, *KRAS* or *BRAF*. Using affinity purification and mass spectrometry, we discovered that erastin acts through mitochondrial voltage-dependent anion channels (VDACs)—a novel target for anti-cancer drugs. We show that erastin treatment of cells harbouring oncogenic RAS causes the appearance of oxidative species and subsequent death through an oxidative, non-apoptotic mechanism. RNA-interference-mediated knockdown of VDAC2 or VDAC3 caused resistance to erastin, implicating these two VDAC isoforms in the mechanism of action of erastin. Moreover, using purified mitochondria expressing a single VDAC isoform, we found that erastin alters the permeability of the outer mitochondrial membrane. Finally, using a radiolabelled analogue and a filter-binding assay, we show that erastin binds directly to VDAC2. These results demonstrate that ligands to VDAC proteins can induce non-apoptotic cell death selectively in some tumour cells harbouring activating mutations in the RAS–RAF–MEK pathway.

In a screen of about 24,000 compounds, we discovered erastin, which induces rapid death in engineered human tumour cells (BJ-TERT/LT/ST/RAS[V12] cells, ref. 2) with oncogenic v-Ha-ras Harvey rat sarcoma viral oncogene homologue (*HRAS*)[V12], but not in isogenic, non-tumorigenic cells lacking oncogenic RAS (BJ-TERT/LT/ST cells) (Fig. 1a, Supplementary Fig. 1 and ref. 3). This cell death was not dependent on the rate of cell division, nor was it idiosyncratic to these cells (Fig. 1a and Supplementary Fig. 2), because cell lines engineered in a similar way responded similarly.

We found that erastin-treated cells did not display changes in nuclear morphology characteristic of apoptosis (Fig. 1c, ref. 3). However, imaging by electron microscopy did reveal changes in mitochondrial morphology, such as loss of structural integrity (Fig. 1b). These mitochondrial morphological changes were not observed in response to staurosporine, hydrogen peroxide or rapamycin—compounds that induce apoptosis, necrosis and autophagy, respectively (Fig. 1b and data not shown).

Given that erastin is a new compound found in a cell-based screen, we had no insight into its mechanism of action. We used a two-pronged approach to define the mechanism, involving, first, a suppressor screen to identify annotated compounds that prevent erastin-induced cell death and, second, an affinity purification approach to identify proteins that mediate the activity of erastin. First, we performed a suppressor screen using a library of about 2,000 biologically active compounds[4] and found that antioxidants (α-tocopherol, butylated hydroxytoluene and β-carotene) prevent erastin-induced death (Fig. 1d, Supplementary Fig. 3). Moreover, we detected generation of an oxidizing species in response to erastin treatment in BJ-TERT/LT/ST/RAS[V12] cells, but not in isogenic BJ-TERT cells (Fig. 1e, Supplementary Fig. 4). Finally, we found that erastin-induced death in the HT-1080 fibrosarcoma cell line was also suppressed by antioxidants (Supplementary Fig. 5).

To characterize the mode of erastin-induced cell death, we looked for features of well characterized death pathways. We determined that the oxidizing species generated in BJ-TERT/LT/ST/RAS[V12] cells in the presence of erastin emanate from mitochondria (see Supplementary Discussion), consistent with the perturbation in mitochondrial morphology. We discovered that the oxidizing species do not cause poly(ADP ribose) polymerase 1 (PARP1) cleavage (Fig. 1f, Supplementary Fig. 6), cytochrome *c* release from mitochondria (Fig. 1g), or pro-caspase-3 cleavage (Fig. 1h)[3,5,6]—all of which are hallmarks of apoptosis, a stereotypical form of cell death activated by many anti-tumour agents[3,7–10] as well as by staurosporine (Fig. 1f–h). Moreover, we looked for these hallmarks in four different cell lines sensitive to erastin; none showed activation of these markers (Fig. 1f, h). Other canonical hallmarks of apoptosis were similarly absent (see Supplementary Information). In summary, these initial studies revealed that erastin induces rapid, oxidative, non-apoptotic death in tumour cells with oncogenic *HRAS*.

To define the genetic basis of the selective lethality of erastin, we used a lentiviral-based RNA interference system[11]. We originally discovered erastin in a screen for oncogenic-*HRAS*-selective lethal compounds. However, v-Ki-ras2 Kirsten rat sarcoma viral oncogene homologue (*KRAS*) is more frequently mutated in human cancers than *HRAS*[12]. Selective toxicity in mutant-KRAS-expressing cell lines would broaden the applicability of erastin as a therapeutic. Thus, we tested whether erastin was selectively lethal to tumour cells harbouring oncogenic *KRAS*, and whether this lethality could be arrested by knockdown of KRAS. We found that a lung carcinoma cell line (Calu-1) with an activating mutation in *KRAS* was sensitive to erastin (half-maximal inhibitory concentration, $IC_{50} = 4\,\mu M$; Fig. 2a); when infected with lentiviral constructs expressing two different short hairpin RNAs (shRNAs) targeting

KRAS (Supplementary Table 4), these cells exhibited resistance to erastin (Fig. 2a, b).

RAS proteins are known to modulate many downstream pathways, and genetic lesions in these pathways are associated with many cancer types[12]. To clarify the connection between erastin and oncogenic RAS signalling, we sought evidence that erastin acts in a manner that is specific to cells with activated RAS–RAF–MEK signalling (Supplementary Table 1 and Supplementary Discussion). One cell line with moderate sensitivity to erastin was A-673 (Supplementary Table 1), containing an activating V600E mutation in v-raf murine sarcoma viral oncogene homologue B1 (BRAF)—a direct target of RAS[13]. To determine whether the activating mutation in BRAF influences erastin sensitivity, we created two different shRNAs targeting BRAF messenger RNA (Supplementary Table 4). We found that A-673 cells containing either of these constructs were resistant to erastin (Fig. 2c–e). Moreover, co-expression of a non-targetable V600E mutant BRAF partially restored sensitivity of these cells to erastin (Supplementary Fig. 7).

To confirm that activated RAS–RAF–MEK signalling renders other tumour cells sensitive to erastin, we examined the effect of mitogen-activated protein kinase (MAPK)/extracellular signal-regulated kinase (ERK) kinase 1/2 (MEK1/2) inhibitors on erastin sensitivity. All three inhibitors caused erastin resistance in both BJ-TERT/LT/ST/RAS^{V12} and HT-1080 cells, with activating mutations in HRAS and NRAS, respectively (Fig. 2f and Supplementary Fig. 8; Supplementary Table 2 shows the effect of these MEK inhibitors alone on cell viability). Finally, we found a modest correlation between ERK1/2 phosphorylation status and erastin sensitivity in 12 sarcoma cell lines (Table 1). In summary, KRAS and BRAF knockdown, MEK inhibition, and analysis of ERK1/2 phosphorylation status together suggest that erastin contains a degree of selectivity for cells in which the RAS–RAF–MEK pathway is constitutively activated.

For the second prong of our approach to defining the mechanism of action of erastin (affinity-based target identification), we synthesized erastin analogues that could be linked to a solid-phase resin for biochemical purification of potential targets. We found that replacement of the p-chloro substituent in erastin with the aminomethyl group necessary for linkage to a resin resulted in an analogue (erastin A6, Fig. 2g) that, though less potent, retained the ability to kill BJ-TERT/LT/ST/RAS^{V12} cells, but not BJ-TERT cells (Supplementary Fig. 9). We also identified a suitable analogue (erastin B2, Supplementary Information) that lacked activity (Fig. 2g and Supplementary Fig. 9), and thus could serve as a negative control for target purification.

We immobilized erastin A6 and erastin B2 on solid-phase resin and sought proteins that interact with A6, but not B2. Using BJ-TERT/LT/ST/RAS^{V12} cell lysates, we identified all three isoforms of the human mitochondrial voltage-dependent anion channels (VDAC1, VDAC2 and VDAC3) on the A6 resin, but only VDAC1 on the B2 resin (Supplementary Table 3, 7–14). Using BJ-TERT cell lysates, we identified a small amount of VDAC1 on the A6 resin, but none of the VDACs on the B2 resin. Thus, it appears that erastin A6 isolates VDAC2 and VDAC3 more efficiently than does erastin B2. Furthermore, the finding that erastin pulls down a mitochondrial protein (VDAC) is consistent with observations that erastin induces mitochondria-driven oxidative death.

VDACs (also known as eukaryotic porins) are membrane-spanning channels that facilitate transmembrane transport of ions
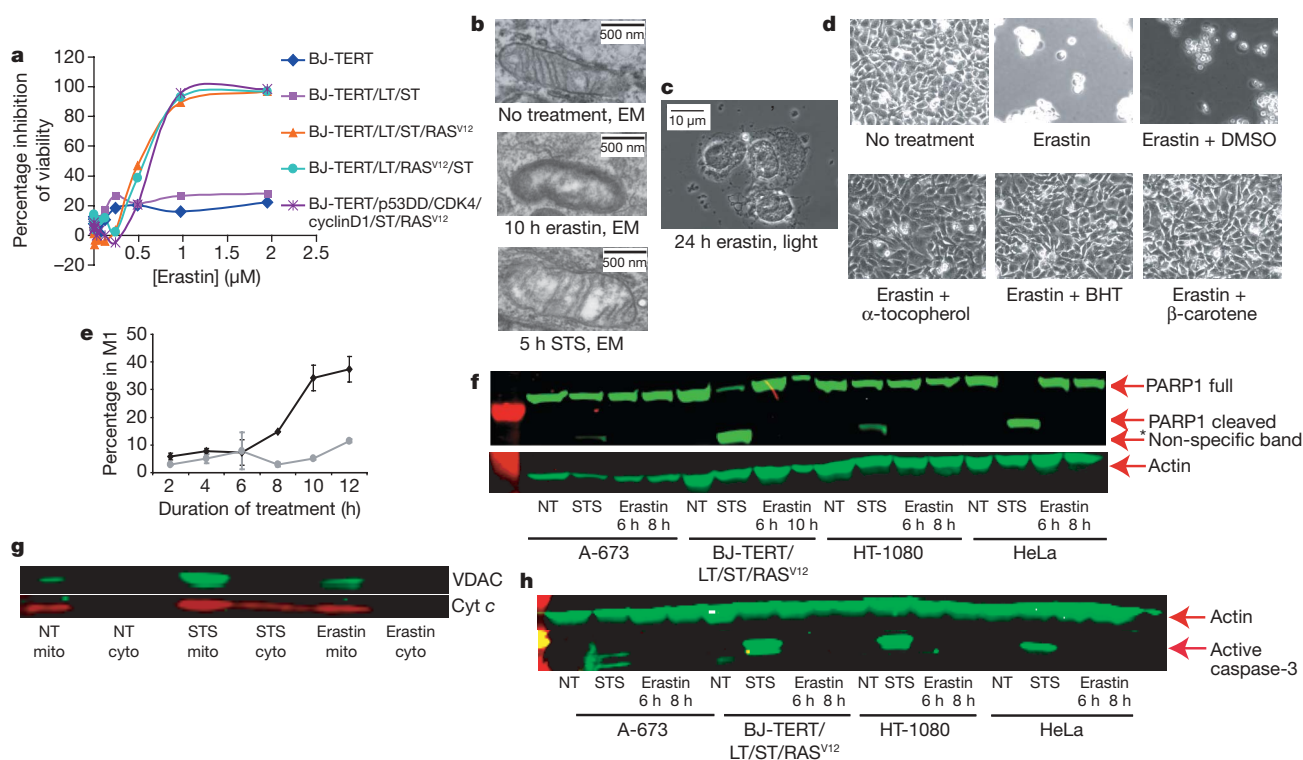

Figure 1 | Erastin activates a rapid, oxidative, non-apoptotic cell death process. a, HRAS^{V12}-expressing cell lines are sensitive to erastin, whereas isogenic lines lacking HRAS^{V12} are resistant, as determined by Trypan blue exclusion; the graph is a representative outcome of multiple independent experiments. **b**, Transmission electron microscopy images (×20,000) of BJ-TERT/LT/ST/RAS^{V12} mitochondria after cells were treated with nothing, erastin (37 μM for 10 h) or staurosporine (STS, 1 μM for 5 h). **c**, Phase-contrast photograph of BJ-TERT/LT/ST/RAS^{V12} cells 24 h after 9 μM erastin treatment indicates that nuclei are intact after cell death. **d**, Anti-oxidants suppress erastin-induced death in BJ-TERT/LT/ST/RAS^{V12} cells. BHT, butylated hydroxytoluene; DMSO, dimethylsulphoxide. **e**, Level of intracellular oxidative species in BJ-TERT/LT/ST/RAS^{V12} (black line) or BJ-TERT (grey line) cells treated with 4.6 μM erastin. y axis, percentage of cells exhibiting dichlorofluorescein (DCF) fluorescence within region of interest, M1, as measured by flow cytometry; error bars, one standard deviation, n = 2. **f**, PARP1 cleavage is not seen during erastin-induced cell death in A-673, HT-1080 and HeLa cells. NT, no treatment. **g**, STS, but not erastin, induces cytochrome c (cyt c) release from BJ-TERT/LT/ST/RAS^{V12} mitochondria; mitochondrial fraction, mito; cytosolic fraction, cyto. **h**, Pro-caspase-3 is not cleaved in response to erastin.
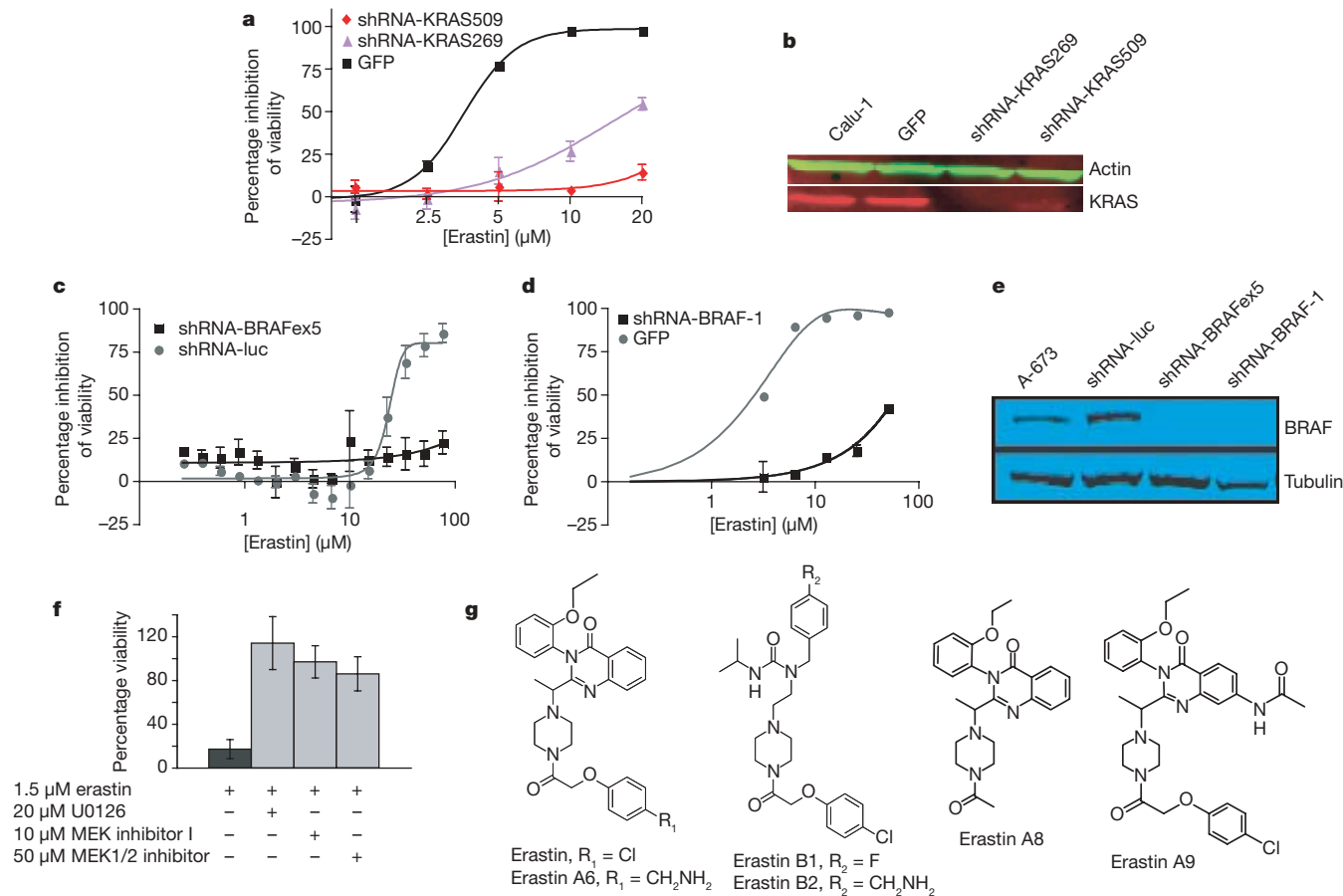
Figure 2 | Erastin lethality is dependent on the RAS–RAF–MEK pathway.
a, Calu-1 cells infected with lentivirus containing shRNAs targeting KRAS
were resistant to erastin-induced lethality as quantified by way of comparison
with green fluorescent protein (GFP) control in Trypan blue exclusion assay.
Sequences of shRNAs are indicated by starting nucleotide in the KRAS mRNA
coding sequence. **b,** KRAS knockdown was confirmed by western blot
analysis. **c, d,** A-673 cells were infected with lentivirus expressing indicated
shRNAs or a control GFP plasmid. Cells were treated with erastin for 24 h;
percentage inhibition of viability (y axis) was measured using **c,** Alamar blue
and **d,** Trypan blue. Luc, luciferase; BRAFex5, exon 5 of *BRAF* transcript.
e, BRAF knockdown was confirmed by western blot analysis. **f,** 48 h treatment
with MEK inhibitors (U0126, Sigma; MEK inhibitor 1, Calbiochem; MEK1/2
inhibitor, Calbiochem) prevents erastin-induced lethality in BJ-TERT/LT/
ST/RAS^{V12} cells; percentage viability (y axis) was determined using Trypan
blue. **g,** Structures of erastin and related analogues. All error bars in Fig. 2
represent one standard deviation; $n = 2$ or 3.

and metabolites[14,15], most notably across the outer mitochondrial
membrane[16]. It has been demonstrated that VDACs are gated by
membrane voltage, at least *in vitro* (Supplementary Discussion): in
the closed state, ions, but not small molecule metabolites, can pen-
etrate VDAC pores[17]; in the open state, both ions and metabolites
pass through VDAC channels. In addition, the closed state is cation-
selective, whereas the open state is anion-selective.

Having identified VDACs as a potential target of erastin, we sought
evidence that altered expression of VDACs contributes to altered
erastin sensitivity. To determine whether VDACs are upregulated
in response to oncogenic *HRAS*, we measured VDAC abundance in
the BJ cell series (see ref. 2 and Supplementary Discussion for engine-
ering and genetics of BJ cell series). In BJ-TERT/LT/ST/RAS^{V12} cells,
the total amount of VDAC protein is increased (Fig. 3a and Sup-
plementary Fig. 10). These results suggest that erastin acts by a gain-
of-function mechanism, and that cells with more VDAC protein are
more sensitive to erastin, although other aspects of cellular physi-
ology may also be relevant.

Next, using two-dimensional gel electrophoresis to evaluate pro-
tein expression in BJ-TERT/LT/ST/RAS^{V12} cells (Supplementary
Fig. 11), we found that, after 8 h of erastin treatment, VDAC3 was
no longer detectable, and, after 10 h, VDAC2 became undetectable
(Fig. 3b). Doxorubicin and camptothecin are examples of agents that
act by a gain-of-function mechanism on their molecular targets,
topoisomerase IIα and topoisomerase I, respectively[18]. It may be that
a cellular response to erastin is downregulation of VDAC2/3 after

lethal oxidative species have been generated, as occurs with camp-
tothecin and topoisomerase I following DNA damage. The fact that
VDAC1 is still present at later time points suggests that the loss of
VDAC2/3 is not simply caused by loss of mitochondria.

To test the gain-of-function hypothesis, we reduced VDAC pro-
tein levels using lentiviral shRNA expression[11]. We created multiple
shRNA constructs targeting each VDAC isoform (Supplementary
Table 4 and Supplementary Fig. 12) and tested their effects on cell
sensitivity to erastin (Supplementary Figs 13–15). We found that
knockdown of VDAC3 caused significant resistance to erastin (Fig.
3c, d and Supplementary Fig. 15). We also observed some degree of

Table 1 | Correlation between erastin sensitivity and phospho-ERK level

Human cell line	Erastin sensitivity (%)	Phospho-ERK1/2
A-673	54	0.66
BJ-TERT	22	0.09
BJ-TERT/LT/ST/RAS^{V12}	100	0.92
EWS 502	42	0.12
HL-60	0	0.10
HT-1080	98	0.53
SK-ES-1	96	0.25
SK-N-MC	95	0.05
SW 872	0	0.12
TC 32	88	0.12
TC 71	92	0.23
U-937	73	0.27

The maximum percentage cell death induced by erastin in each cell line is shown, along with the
level of phospho-ERK1/2 as quantified by western blot (arbitrary units). The correlation is 0.41.

erastin resistance when VDAC2 was knocked down (Fig. 3c, e and Supplementary Fig. 14). In contrast, overexpression of VDAC3 alone in BJ-TERT cells yielded no increase in sensitivity to erastin (Supplementary Fig. 16), suggesting that VDAC3, and to some degree VDAC2, is necessary but not sufficient for sensitivity to erastin and that other downstream features of RAS–RAF–MEK signalling are also needed. Overall, these results are consistent with a gain-of-function mechanism involving erastin and VDAC2/3. Furthermore, this effect is specific to erastin, and not to other lethal compounds: VDAC2-deficient embryonic stem cells have been shown to be more sensitive, not less sensitive, to staurosporine and etoposide[19].

To test the hypothesis that erastin alters mitochondrial outer membrane permeability, we monitored the function of VDACs using purified mitochondria from yeast engineered to express a single mouse VDAC isoform in place of yeast VDAC[20]. A previous report demonstrated that the rate of NADH uptake through the outer

membrane of such mitochondria is dependent on the specific VDAC expressed in yeast. We found that erastin treatment yielded a decrease in the rate of NADH oxidation, suggesting a reduced permeability of these mitochondria to NADH when mouse VDAC1 or VDAC2 were expressed (Fig. 3f and Supplementary Fig. 17). We found little NADH oxidation in mitochondria expressing VDAC3, suggesting minimal intrinsic membrane permeability (Supplementary Fig. 17); this is consistent with previous reports that VDAC3 does not gate well *in vitro*[20]. Finally, we found that an inactive analogue of erastin (erastin A8, Fig. 2g and Supplementary Fig. 9) had no such effect (Fig. 3f and Supplementary Fig. 17). These results suggest that erastin affects VDAC gating, possibly switching its ion selectivity and allowing cationic species into mitochondria.

Having demonstrated interactions between erastin and VDAC using affinity-based target identification and VDAC functional assays, we explored the direct binding of erastin to VDACs. Using modified versions of previously reported protocols, we isolated VDAC2 from *Escherichia coli* for use in a competition binding experiment[21,22] using a radiolabelled analogue (erastin A9). The results demonstrate that the cold RAS-selective lethal erastin A9 (IC_{50} = 1.9 μM, Supplementary Fig. 9), unlike inactive erastin A8, directly binds to VDAC2 (dissociation constant, K_d = 112 nM; Fig. 3g), in the process competing off radiolabelled erastin A9.

The data presented herein are consistent with a model in which erastin interacts with VDAC proteins to induce mitochondrial dysfunction, release of oxidative species and, ultimately, non-apoptotic, oxidative cell death. This process has a degree of selectivity for cells with activated RAS–RAF–MEK signalling. These results demonstrate that it is feasible to discover oncogene-selective compounds and to use them to clarify oncogene-related cell death mechanisms.

METHODS SUMMARY

VDAC identification using pull-down assay. Erastin A6 and B2 were linked to a solid-phase resin, which was then incubated with BJ-TERT/LT/ST/RAS[V12] or BJ-TERT cell lysate and washed before protein was eluted and then digested as described[23]. Reverse-phase high-performance liquid chromatography was performed before samples were analysed using both a 4700 Proteomics Analyser matrix-assisted laser desorption/ionization-time of flight (TOF)/TOF (TOF/TOF; Applied Biosystems) and a Q Trap (AB/MDS Sciex). Tandem mass spectrometry (MS/MS) data was then compared against either the corrected NCBInr protein sequence database or the HumanNR database (http://www.ncbi.nlm.nih.gov/). GPS Explorer (Applied Biosystems) was used for submitting data acquired from the TOF/TOF for database searching.

Knockdown using lentiviral shRNAs. HT-1080 and Calu-1 cells were infected with lentiviruses expressing shRNAs targeting VDAC and KRAS, respectively (Supplementary Table 4). A-673 cells were infected with retroviruses[24] expressing shRNAs against either BRAF or luciferase (Supplementary Table 4).

NADH oxidation assay. NADH oxidation in the mitochondria was measured by resuspending mitochondria isolated from yeast in 25 μM NADH, with or without erastin, and monitoring absorbance at λ = 340 nm (ref. 20). As a control for mitochondrial intactness, parallel assays were run using hypotonically shocked mitochondria.

VDAC2 binding assay. VDAC2 protein was isolated from *E. coli* using a modified version of a previously described protocol[22]. To assay direct binding of erastin analogues, 40 μg of purified VDAC2 was incubated in the presence of 20 μM radiolabelled erastin A9 and serial dilutions of unlabelled erastin A9 or erastin A8. The mixture was then deposited onto a binding filter using vacuum filtration. After rinsing, radioactivity was detected on a liquid scintillation counter (LKB Wallac 1,211 RACKBETA).

Full protocols. For detailed methods, which additionally include cell culture, western blotting, cell viability assays, PARP cleavage, cytochrome *c* release, oxidative species detection, transmission electron microscopy, VDAC3 overexpression, PCR with reverse transcription and quantitative PCR, see Methods.
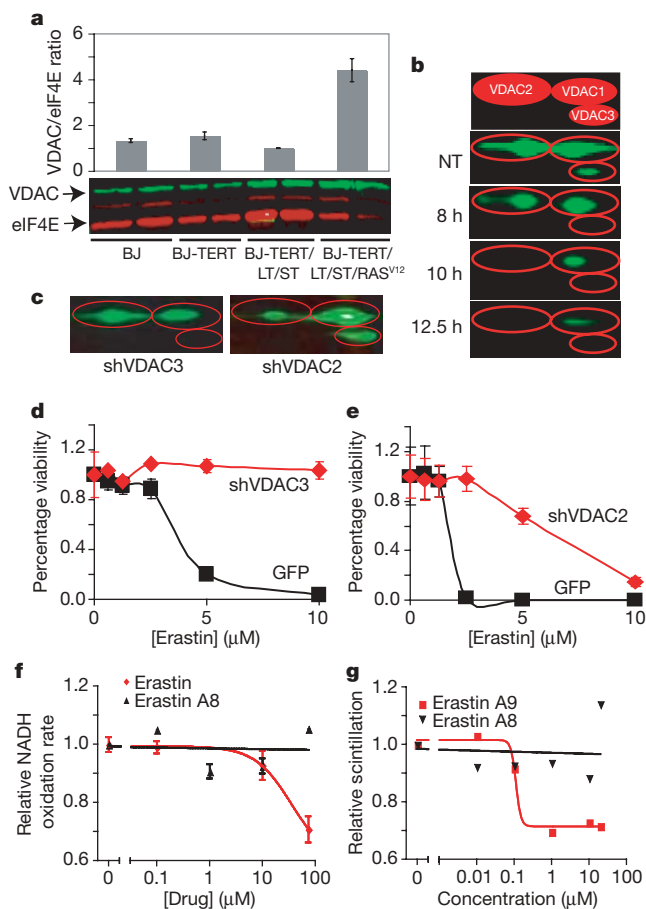
Figure 3 | Erastin compounds act through VDACs. a, VDAC/eukaryotic initiation factor 4E (eIF4E) protein ratio in engineered BJ-derived cells as quantified using western blot. **b**, BJ-TERT/LT/ST/RAS[V12] cells were treated with erastin and harvested at indicated time points for quantitative two-dimensional western blot. The top panel is an illustration of VDAC isoforms separated by two-dimensional gel electrophoresis. **c**, Isoform-specific knockdown of VDAC in HT-1080 cells infected with virus expressing either VDAC3- or VDAC2-targeted shRNA plasmid (shVDAC3 or shVDAC2) was confirmed using two-dimensional protein gels. **d, e**, These cells were then treated with erastin dilutions, and viability relative to no treatment (*y* axis) was determined using Trypan blue exclusion and compared to an identical process using a GFP control plasmid. **f**, Rate of NADH oxidation, normalized to no treatment, in mitochondria purified from VDAC-knockout yeast expressing murine VDAC2 was determined in the presence of erastin (red) or an inactive analogue, erastin A8 (black). **g**, Direct binding to VDAC2 was assayed using tritium-labelled erastin A9 in competition with unlabelled erastin A9 (red) or erastin A8 (black). All error bars in Fig. 3 represent one standard deviation, *n* = 2 or 3.

1. Kaelin, W. G. The concept of synthetic lethality in the context of anticancer therapy. *Nature Rev. Cancer* **5**, 689–698 (2005).

2. Hahn, W. C. *et al.* Creation of human tumour cells with defined genetic elements. *Nature* **400**, 464–468 (1999).

3. Dolma, S., Lessnick, S. L., Hahn, W. C. & Stockwell, B. R. Identification of genotype-selective antitumor agents using synthetic lethal chemical screening in engineered human tumor cells. *Cancer Cell* **3**, 285–296 (2003).

4. Root, D. E., Flaherty, S. P., Kelley, B. P. & Stockwell, B. R. Biological mechanism profiling using an annotated compound library. *Chem. Biol.* **10**, 881–892 (2003).

5. Song, Z. & Steller, H. Death by design: mechanism and control of apoptosis. *Trends Cell Biol.* **9**, M49–M52 (1999).

6. Majno, G. & Joris, I. Apoptosis, oncosis, and necrosis. An overview of cell death. *Am. J. Pathol.* **146**, 3–15 (1995).

7. Wyllie, A. H. Glucocorticoid-induced thymocyte apoptosis is associated with endogenous endonuclease activation. *Nature* **284**, 555–556 (1980).

8. Kerr, J. F., Wyllie, A. H. & Currie, A. R. Apoptosis: a basic biological phenomenon with wide-ranging implications in tissue kinetics. *Br. J. Cancer* **26**, 239–257 (1972).

9. Martin, S. J. *et al.* Early redistribution of plasma membrane phosphatidylserine is a general feature of apoptosis regardless of the initiating stimulus: inhibition by overexpression of Bcl-2 and Abl. *J. Exp. Med.* **182**, 1545–1556 (1995).

10. Yuan, J., Shaham, S., Ledoux, S., Ellis, H. M. & Horvitz, H. R. The *C. elegans* cell death gene ced-3 encodes a protein similar to mammalian interleukin-1 beta-converting enzyme. *Cell* **75**, 641–652 (1993).

11. Moffat, J. *et al.* A lentiviral RNAi library for human and mouse genes applied to an arrayed viral high-content screen. *Cell* **124**, 1283–1298 (2006).

12. Downward, J. Targeting RAS signalling pathways in cancer therapy. *Nature Rev. Cancer* **3**, 11–22 (2003).

13. Davies, H. *et al.* Mutations of the *BRAF* gene in human cancer. *Nature* **417**, 949–954 (2002).

14. Graham, B. H. & Craigen, W. J. Genetic approaches to analyzing mitochondrial outer membrane permeability. *Curr. Top. Dev. Biol.* **59**, 87–118 (2004).

15. Baker, M. A., Lane, D. J., Ly, J. D., De Pinto, V. & Lawen, A. VDAC1 is a transplasma membrane NADH-ferricyanide reductase. *J. Biol. Chem.* **279**, 4811–4819 (2004).

16. Rostovtseva, T. & Colombini, M. ATP flux is controlled by a voltage-gated channel from the mitochondrial outer membrane. *J. Biol. Chem.* **271**, 28006–28008 (1996).

17. Mannella, C. A. Minireview: on the structure and gating mechanism of the mitochondrial channel, VDAC. *J. Bioenerg. Biomembr.* **29**, 525–531 (1997).

18. Beck, W. T. & Danks, M. K. Mechanisms of resistance to drugs that inhibit DNA topoisomerases. *Semin. Cancer Biol.* **2**, 235–244 (1991).

19. Cheng, E. H., Sheiko, T. V., Fisher, J. K., Craigen, W. J. & Korsmeyer, S. J. VDAC2 inhibits BAK activation and mitochondrial apoptosis. *Science* **301**, 513–517 (2003).

20. Xu, X., Decker, W., Sampson, M. J., Craigen, W. J. & Colombini, M. Mouse VDAC isoforms expressed in yeast: channel properties and their roles in mitochondrial outer membrane permeability. *J. Membr. Biol.* **170**, 89–102 (1999).

21. Poyurovsky, M. V. *et al.* Nucleotide binding by the Mdm2 RING domain facilitates Arf-independent Mdm2 nucleolar localization. *Mol. Cell* **12**, 875–887 (2003).

22. Koppel, D. A. *et al.* Bacterial expression and characterization of the mitochondrial outer membrane channel. Effects of n-terminal modifications. *J. Biol. Chem.* **273**, 13794–13800 (1998).

23. Zhen, Y. *et al.* Development of an LC-MALDI method for the analysis of protein complexes. *J. Am. Soc. Mass Spectrom.* **15**, 803–822 (2004).

24. Sage, J., Miller, A. L., Perez-Mancera, P. A., Wysocki, J. M. & Jacks, T. Acute mutation of retinoblastoma gene function is sufficient for cell cycle re-entry. *Nature* **424**, 223–228 (2003).

METHODS

Cell culture and western blotting. BJ-TERT/LT/ST/RAS^{V12} cells were cultured as described in ref. 3. Other cell lines were grown according to specifications of the American Type Culture Collection. For western blots, medium was aspirated and each dish was washed twice with 10 ml ice-cold PBS. Cells were lysed with 200 μl buffer (50 mM HEPES, 40 mM NaCl, 2 mM EDTA, 0.5% Triton-X, 1.5 mM sodium orthovanadate, 50 mM NaF, 10 mM sodium pyrophosphate, 10 mM sodium β-glycerophosphate and protease inhibitor tablet (Roche), (pH 7.4)). For one-dimensional western blots, samples were separated using SDS–polyacrylamide gel electrophoresis; for two-dimensional western blots, samples were prepared using the ZOOM IPGRunner System (Invitrogen). Following separation, samples were then transferred to a polyvinylidene difluoride membrane, blocked for 1 h at room temperature in Licor Odyssey Blocking Buffer and incubated with the necessary primary and secondary antibodies: anti-VDAC1 (Abcam, ab3434), anti-VDAC1 (Calbiochem, 529534), anti-VDAC2 (Abcam, ab22170), anti-eIF4E (Santa Cruz Biotechnology, sc-9976), anti-α-tubulin (Sigma, T6199), anti-actin (Santa Cruz Biotechnology, 1616R), IRDye 800 goat anti-rabbit antibody (Rockland Immunochemicals, 611-132-122), Alexa Fluor 680 goat anti-mouse (Molecular Probes, A21058), PathScan Multiplex Western Cocktail I Kit (Cell Signalling Technology) and anti-PARP (Abcam, ab105). Membranes were scanned using the Licor Odyssey Imaging System.

PARP cleavage and cytochrome c release. BJ-TERT/LT/ST/RAS^{V12} cells were seeded in polystyrene 100 × 20 mm dishes (Falcon, 353003) in 10 ml medium. 3×10^6 cells were seeded in each dish. After overnight incubation at 37 °C with 5% CO$_2$, BJ-TERT/LT/ST/RAS^{V12} cells were treated with nothing, staurosporine (1 μM) for 6 h, camptothecin (1 μM) for 18 h, or erastin (20 μg ml^{-1}) for 6, 10, 12, 12.5, 13, 14, 18 or 26 h, and prepared for western blotting. For the cytochrome c release assay, cells were washed with 10 ml ice-cold PBS, suspended in 120 μl buffer (300 mM sucrose, 0.1% BSA, 10 mM HEPES (pH 7.5), 10 mM KCl, 1.5 mM MgCl$_2$, 1 mM EGTA, 1 mM EDTA, 1 mM dithiothreitol (DTT), 2 mM phenylmethanesulphonyl fluoride and one protease inhibitor tablet (Roche)) and incubated on ice for 15 min. Cells were lysed by passing them through a 25-gauge needle (5 strokes). Cell lysates were centrifuged at 400g for 5 min at 4 °C to remove the nuclear fraction. Mitochondria were removed from the soluble cytosolic fraction by pelleting at 10,500g. Supernatant and mitochondrial pellets were solubilized in SDS–polyacrylamide gel electrophoresis loading buffer and analysed by western blotting.

Oxidative species detection. 2′7′-dichlorodihydrofluorescein diacetate (H$_2$DCF-DA, Molecular Probes) was used to measure oxidative species by flow cytometry. Non-fluorescent H$_2$DCF-DA was cleaved by endogenous esterases and then was oxidized to generate fluorescent DCF. BJ-TERT/LT/ST/RAS^{V12} and BJ-TERT cells were seeded at 3×10^5 cells per dish in 60 mm dishes and allowed to grow overnight. Cells were treated with 4.6 μM erastin for 2, 4, 6, 8, 10 and 12 h. For each time point, controls were maintained for untreated cells and also for positive control (treated directly with 500 μM hydrogen peroxide for 5 min). Cells were incubated with 10 μM H$_2$DCF-DA for 10 min, harvested by trypsinization, washed twice with cold PBS, resuspended in 100 μl PBS and incubated with 5 μl of 50 μg ml^{-1} propidium iodide for 10 min. 400 μl PBS was added and the solution was analysed by flow cytometry (FACSCalibur, Becton-Dickinson). FL1-H indicates arbitrary units of DCF fluorescence detected.

VDAC pull-downs. Cultures of BJ-TERT and BJ-TERT/LT/ST/RAS^{V12} cells (ten 150-mm plates) were washed with PBS, lysed in 25 mM HEPES (pH 7.5), 150 mM NaCl, 1% NP-40, 10 mM MgCl$_2$, 1 mM EDTA, 10% glycerol, 1 mM DTT and protease inhibitor cocktail. Total protein concentration was determined using a Bradford colorimetric assay.

Erastin A6 and B2 were dissolved in DMSO at 10 mg ml^{-1}. 100 μl AffiGel-10 (BioRad) was washed and resuspended in 400 μl DMSO. 10 μl compound and 3 μl 1:100 dilution of triethylamine in DMSO were added. The suspension was incubated at room temperature for 14 h, washed (1 ml per wash) five times in DMSO, three times in PBS, resuspended in 3 M ethanolamine in PBS, incubated 1 h at room temperature, washed five times in PBS and resuspended in 200 μl PBS. For the pull-down experiments, 50 μl of the A6 or B2 gel slurry was washed with binding buffer (0.1 M KCl, 20 mM HEPES (pH 7.6), 0.1 mM EDTA, 10% glycerol, 0.1% NP-40, 1 mM DTT, 0.25 mM phenylmethylsulphonyl fluoride) and incubated with 1 ml cell lysate (2 mg ml^{-1} for 1.5 h at 4 °C), washed with binding buffer, washed three times with high salt buffer (0.35 M KCl, 20 mM HEPES (pH 7.6), 0.1 mM EDTA, 10% glycerol, 0.1% NP-40, 1 mM DTT, 0.25 mM phenylmethylsulphonyl fluoride), washed with binding buffer, and eluted twice with 50 μl elution buffer (binding buffer with 0.8% N-lauroyl sarkosine). Proteins from the supernatant were precipitated with 400 μl ethanol, sedimented by centrifugation (16,800g) and digested as described[23]. Reverse-phase high-performance liquid chromatography was performed using a nano LC system (Dionex): a 75 μm × 150 mm column, a Famos autosampler, a Switchos II

system and an UltiMate binary pumping module. Samples were analysed using both a 4700 Proteomics Analyser MALDI-TOF/TOF (TOF/TOF; Applied Biosystems) and a Q Trap (AB/MDS Sciex), and the peptide level data were combined. To construct the databases used for protein identification, the following steps were performed: the NCBInr protein sequence FASTA file was downloaded, the GI numbers (sequence version identification) were updated, and the missing or incorrectly annotated taxonomies were fixed by referencing them to the NCBI taxonomy index (index of GI number versus species). The human subset of proteins in the database was extracted into a separate database (HumanNR). All protein sequences in HumanNR were matched to the corresponding protein in RefSeq using BLAST[25]. MS/MS data obtained from the TOF/TOF and Q Trap were searched using Mascot (Matrix Sciences, London, UK). All searches were performed against either the corrected NCBInr protein sequence database or the HumanNR database. GPS Explorer (Applied Biosystems) was used for submitting data acquired from the TOF/TOF for database searching. The Mascot-based search was performed using the default settings for the specific instrument type as supplied by Matrix Science, except that ions with scores below ten were excluded from the results.

The spectra of the peptides identified in the automatic data analysis were manually inspected for the quality of the corresponding spectra and for consistency with the obtained results. Only high quality spectra and results with a peptide score of 20 or higher were accepted and used for the identification of proteins.

Transmission electron microscopy of BJ-TERT/LT/ST/RAS^{V12} cells treated with erastin. Cells were incubated for 10 h in the presence of erastin (20 μg ml^{-1}) or nothing, fixed with 2.5% glutaraldehyde in 0.1 M Sorenson's buffer (0.1 M H$_2$PO$_4$, 0.1 M HPO$_4$ (pH 7.2)) for at least 1 h, and then treated with 1% OsO$_4$ in 0.1 M Sorenson's buffer for 1 h. Enblock staining used 1% tannic acid. After dehydration through an ethanol series, cells were embedded in Lx-112 (Ladd Research Industries) and Embed-812 (EMS). Thin sections were cut on an MT-7000 ultramicrotome, stained with 1% uranyl acetate and 0.4% lead citrate, and examined under a Jeol JEM-1200 EXII electron microscope. Pictures were taken on an ORCA-HR digital camera (Hamamatsu) at ~20,000-fold magnification, and measurements were made using the AMT Image Capture Engine.

Knockdown using lentiviral shRNAs. VDACs, KRAS and BRAF were knocked down in HT-1080, Calu-1 and A-673 cells, respectively, using shRNA lentiviral vectors (Supplementary Table 4). On day 1, 293T cells were seeded in 10 cm tissue culture dishes (2×10^6 cells per dish); on day 2, shRNA-plasmid construct (pLKO.1 vector for VDAC- and KRAS-targeting constructs; pSIRIPP[24] for BRAF- or luciferase-targeting constructs; Supplementary Table 4) and the pΔ8.9 and pVSV-G helper plasmids were co-transfected into the 293T cells using FuGENE 6 Transfection Reagent (Roche); on day 3, the medium was changed; on day 4, the supernatant, containing virus, was transferred to target cells in 10 cm tissue culture dishes (1×10^6 cells per dish); on day 5, cells were transferred to 175 cm^2 flasks and medium was supplemented with puromycin (1.5 μg ml^{-1}); on days 6 and 7, medium was changed and again supplemented with puromycin; on day 8, samples were harvested for western blot and quantitative PCR with reverse transcription, or reseeded in 6-well format (5×10^5 cells per well), in duplicate, and treated with erastin dilutions. All cells were cultured at 37 °C, 5% CO$_2$, in growth media as recommended by ATCC (American Type Culture Collection).

Overexpression of VDAC3 using lentiviral constructs. VDAC3 was over-expressed in BJ-TERT cells using a human ORF clone (Invitrogen) recombined into the pLENTi6/V5-DEST lentiviral vector (Invitrogen). On day 1, 293T cells were seeded in 10 cm tissue culture dishes (2×10^6 cells per dish); on day 2, the VDAC3 construct and the pΔ8.9 and pVSV-G helper plasmids were co-transfected into the 293T cells using FuGENE 6 Transfection Reagent (Roche); on day 3, the medium was changed; on day 4, the supernatant, containing virus, was transferred to BJ-TERT cells in 10 cm tissue-culture dishes (1×10^6 cells per dish); on day 5, cells were transferred to 175 cm^2 flasks and medium was supplemented with blasticidin (5 μg ml^{-1}); on days 6 and 7, medium was changed and again supplemented with blasticidin. These cells were maintained in selection medium for 12 days before samples were harvested for future assay.

Reverse transcription and quantitative PCR. Total RNA was isolated from cells using RNeasy Mini Kit (Qiagen). Reverse transcription was performed on 2 μg isolated RNA using Taqman Reverse Transcription Reagents (Applied Biosystems). The ABI Prism 7,300 was then used for quantitative PCR. 20 ng complementary DNA product was mixed with Power SYBR Green PCR Master Mix (Applied Biosystems) and each of the appropriate forward/reverse primer set (Supplementary Table 5). Relative mRNA expression levels were quantified with Sequence Detection Software v1.3.1 (Applied Biosystems).

NADH oxidation assay. NADH oxidation in the mitochondria was measured by resuspending mitochondria isolated from yeast in R-buffer (0.65 M sucrose, 10 mM HEPES (pH 7.5), 10 mM KH$_2$PO$_4$, 5 mM KCl, 5 mM MgCl$_2$) to a final

concentration of $100 \,\mu g \, ml^{-1}$. Mitochondrial concentration was measured by dissolving mitochondria in 0.6% SDS and reading absorbance at $\lambda = 280 \, nm$. The mitochondrial suspension was then incubated with $25 \,\mu M$ NADH, and the absorbance at $\lambda = 340 \, nm$ monitored over a 15 min period. The assay was repeated in the presence of erastin. To assess mitochondrial intactness, a parallel assay was run in which mitochondria were hypotonically shocked before addition of NADH. The mitochondrial pellet was resuspended in distilled H_2O and incubated on ice for 3 min to disrupt the outer mitochondrial membrane; $2 \times$ R-buffer was then added to restore normal osmotic conditions.

Cell viability assays. Trypan blue exclusion: cells were trypsinized, pelleted and resuspended in 1 ml growth media. Trypan blue exclusion analysis was performed using the Vi-CELL Series Cell Viability Analyser 1.01 (Beckman Coulter). Alamar blue metabolism: 10% Alamar blue was added to assay plates, which were then incubated for an additional 16 h. Red fluorescence, resulting from reduction of Alamar blue, was detected on a Victor3 platereader (excitation/emission: 530/590).

VDAC2 binding assay. VDAC2 protein was isolated from *E. coli* using a modified version of the protocol originally described in ref. 22. Bacterial cultures were grown in Luria-Bertani broth containing $50 \, mg \, l^{-1}$ ampicillin to an absorbance of 0.6 ($\lambda = 600 \, nm$), and induced using $0.4 \,\mu M$ isopropylthiogalactoside overnight. Cultures were harvested by centrifugation at $6,000g$ for 10 min. The pellet was then washed with distilled H_2O and resuspended in buffer (20% sucrose, 20 mM Tris buffer (pH 8.0), $50 \,\mu M \, ml^{-1}$ lysozyme) and incubated at $25 \,^{\circ}C$ for 10 min. The lysate was then sonicated for $2 \times 30 \, s$ and centrifuged at $15,000g$ for 20 min. The pellet was resuspended in resuspension buffer (4.5 M guanidine-HCl, 0.1 M NaCl, 20 mM Tris (pH 8.0)) and incubated for 1 h at $25 \,^{\circ}C$. The suspension was then centrifuged (20 min, $15,000g$), and the supernatant was loaded on a Ni-NTA Superflow column (Qiagen) pre-equilibrated with five volumes of resuspension buffer. The column was washed with five column volumes of resuspension buffer containing 10 mM imidazole. The protein was eluted using resuspension buffer containing 225 mM imidazole. The eluate was then dialysed against 0.1 M NaCl, 20 mM Tris (pH 8.0) and 2% LDAO (Fluka) overnight, and then concentrated by means of centrifugation to $4 \, mg \, ml^{-1}$. To assay direct binding of erastin analogues, $40 \,\mu g$ of purified VDAC2 was resuspended in $100 \,\mu l$ of binding buffer (25 mM HEPES (pH 8.0), 0.1% BSA, 7 mM $MgCl_2$, 15 mM NaCl), and then incubated in the presence of $20 \,\mu M$ radiolabelled erastin A9 and serial dilutions of erastin A9 or erastin A8 for 15 min. The mixture was then deposited onto Protran BA85 $0.45 \,\mu M$ binding filters (Whatman) using vacuum filtration. The filter was rinsed 5 times with 1 ml wash buffer (25 mM HEPES, 0.1% BSA), and incubated in 5 ml scintillation liquid (Cytoscint, MP biomedicals). Radioactivity was detected on a LKB Wallac 1211 RACKBETA liquid scintillation counter.

25. Altschul, S. F., Gish, W., Miller, W., Myers, E. W. & Lipman, D. J. Basic local alignment search tool. *J. Mol. Biol.* **215**, 403–410 (1990).